50

INFLUENCE OF PASSAGEWAY FIRES ON VENTILATION FLOWS

C. K. Lee, C. C. Hwang*, J. M. Singer, and R. F. Chaiken

Pittsburgh Mining and Safety Research Center
Bureau of Mines
U. S. Department of the Interior
Pittsburgh, Pennsylvania

ABSTRACT

The influence of passageway fires on ventilation flows was investigated in three horizontal fire tunnels: 1. a laboratory-scale fire tunnel network, 2. a small-scale fire-plume tunnel, and 3. a large-scale simulated mine gallery. Wood was used in the first and third tunnel and gas-burners were used in the second one to generate passageway fires. Experimental measurements included gas mass flow rate, velocity, temperature and pressure in the passageways and exhaust fans. The overall and local effects of the fires were investigated by comparing these measurements obtained before and during the fires. Results show that a passageway fire essentially increases the flow resistances of the passageways of a tunnel flow network by virtue of volatile fuel mass injection and high combustion temperatures. The ventilation air flow rate is consequently throttled to lower values than that before the fire. At severe throttling, reverse flow occurs. Conditions for reverse flow are characterized by two Froude numbers based on gas velocity and density upstream of the fire, and height of the passageway. The Froude numbers and the characteristics of the passageway fire are necessary to analyze mine ventilation/fire interaction and to predict mine ventilation patterns during fires.

INTRODUCTION

As a fire develops in a passageway of an underground mine, it interacts with ventilation air flow and generates aerodynamic disturbances in the ventilation flow. The interaction and disturbance may lead to drastic changes in the ventilation flow pattern, such as throttling of air flow and backing up or reverse flow of hot gases and smoke from the fire into the ventilation air stream. Such effects not only complicate fire-fighting procedures but also present extreme fire hazards in propagating toxic fumes and gases far away from the fire.

In the present work, the influence of passageway fires on ventilation air flows is studied in three horizontal fire tunnels: (1) a laboratory-scale model tunnel network, (2) a small-scale fire-plume tunnel, and (3) a large-scale simulated mine gallery. Gas mass flow rate, velocity, temperature, and pressure were measured before and during the fires in the passageways of the three tunnels. These measurements were used to investigate the flow coupling process among the fires, the ventilation flows and the exhaust fans, fire throttling effects, and reverse flow phenomena. Results suggested techniques for predicting changes in ventilation flow owing to passageway fires.

* Faculty Member, Department of Mechanical Engineering, University of Pittsburgh, Pittsburgh, PA, USA.

EXPERIMENT

Model Tunnel Network

Schematic layouts of the model fire tunnel network and instrumentation are shown in Figs. 1 and 2. Details of the design, instrumentation and operation of the tunnel have been given by Chaiken et al[1,2] and Lee et al[3]. Briefly, the tunnel network consisted of a 0.3 m x 0.3 m (cross section) x 10 m (length) fire duct in parallel with a 0.25 m (diameter) bypass duct. The ignition section of the fire duct was lined on four walls with 0.3 m (height) x 0.15 m (width) x 0.03 m (thickness) oak slabs to form a 0.99 m long wood loading as an ignition source for the wood lining in the test section. The test section was lined on two side walls and the ceiling with oak slabs of

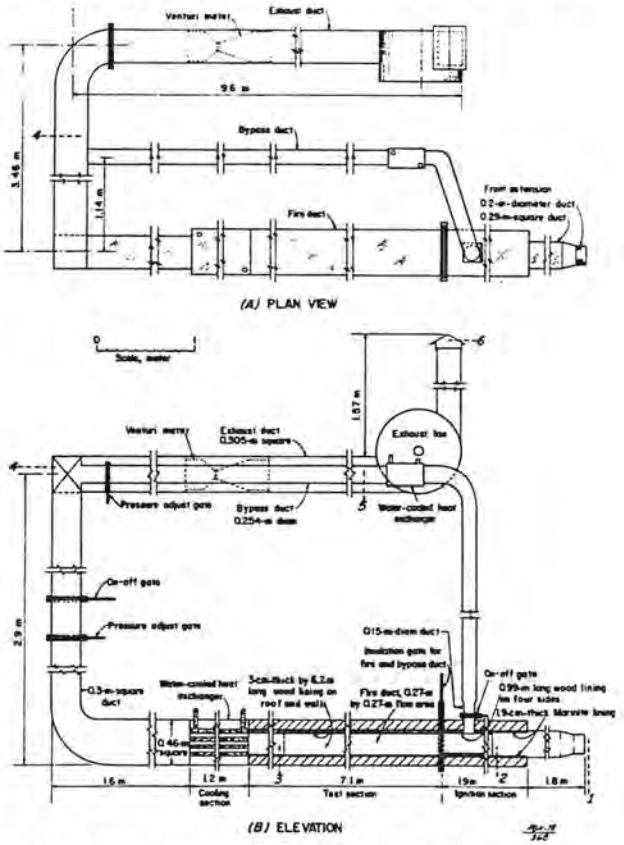

FIGURE 1. Schematic of model tunnel network:
A. Plan view of tunnel network.
B. Vertical cross-section of fire duct and side view of tunnel network.

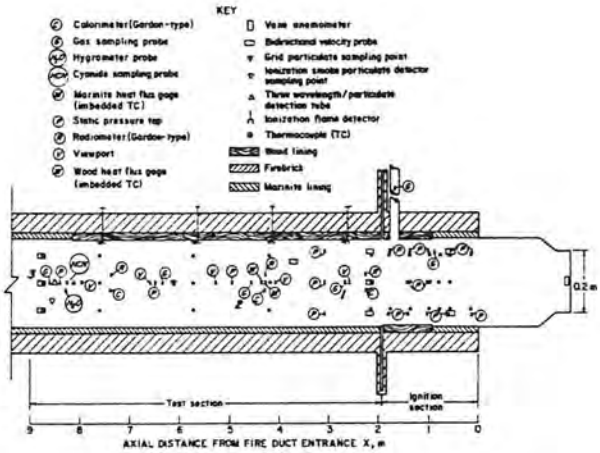

FIGURE 2. Instrumentation of fire duct in tunnel network.

similar size to form a 6.2 m long fuel lining. The ignition and test sections were separated by an insulation gate to ensure thermal and flow isolation of the two sections before fire testing of the wood lining in the test section.

A typical fire experiment was started by initially establishing steady burning of the wood lining in the ignition section. During this time period, ventilation air passed through the ignition section into the bypass duct. After several minutes of steady burning in the ignition section, the ventilation air was directed from the ignition section into the test section of the fire duct by closing and opening of the gates in the two ducts. Through such procedures, the wood lining in the test section was exposed to the ignition source in a controlled manner. After an ignition delay time, flame propagated downstream into the test section; subsequently, the entire fire duct became fully inflamed. During the fire, ventilation air flow rate, fire duct exhaust gas flow rate, and gas temperature and pressure of the tunnel network were measured. Exhaust fan speeds were kept constant as well as varied to study various degrees of fire throttling and reverse flow.

Small-Scale Fire-Plume Tunnel

A schematic layout of the fire-plume tunnel and instrumentation is shown in Fig. 3. Details of the

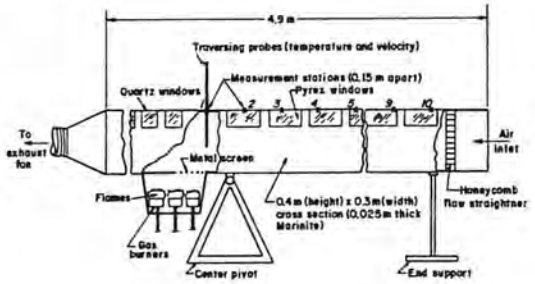

FIGURE 3. Schematic of fire-plume tunnel and instrumentation.

design and operation of the tunnel have been given by Wargo[4]. Briefly, the tunnel was 0.4 m (height) x 0.3 m (width) x 4.9 m (length) and made of Marinite. A fire on the floor was simulated by means of a hot gas plume rising from three premixed gas burners located below the floor of the tunnel. Gas volumetric flow rate and air to gas ratio of the burners could be varied to generate a "fire" of various intensities. Ventilation air flow rate was controlled by a variable-speed blower located at the tunnel entrance. By varying the fire plume intensity and ventilation air velocity, various degrees of fire throttling and reverse flow at steady flow conditions were generated. Details of the stratified reverse flow upstream of the fire plume were investigated by means of velocity and temperature measurements at nine locations showh in Fig. 3.

Full-Scale Simulated Mine Gallery

The overall objective of the full-scale mine gallery fire tests** was to investigate the hazards of timber-set fires and recommend fire safety guidelines to MSHA (Mining Safety and Health Administration) and to the mining industry. One of the areas of investigation was the effect of fire throttling on ventilation air flow.

Figs. 4 and 5 show an overview and a schematic of the gallery facility. Details of the gallery construction and operation have been reported by Buckley et al[5-7]. Basically, the gallery was a T-shaped

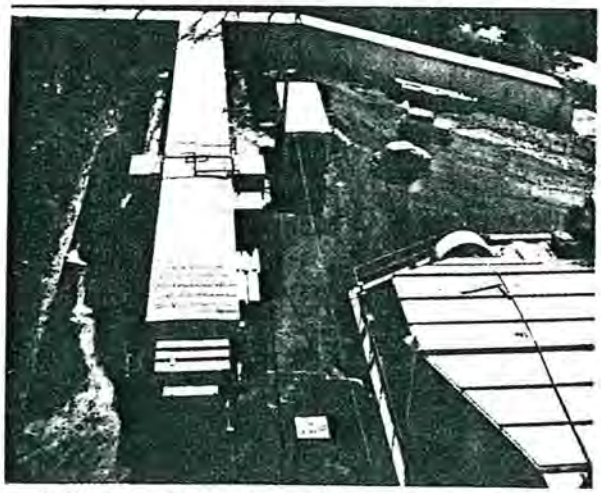

FIGURE 4. Photograph of large-scale simulated mine gallery.

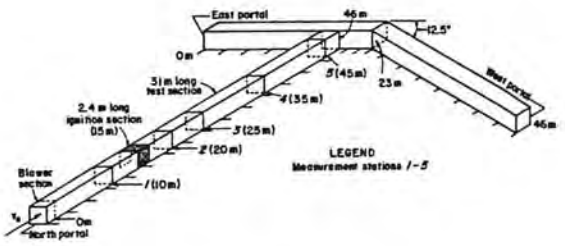

FIGURE 5. Schematic of mine gallery.

** Performed by Factory Mutual Research Corporation, Norwood, Mass., USA.

concrete/brick structure with two passageways of 2.4 m x 2.4 m (cross section) x 46 m (length). One passageway was horizontal and the other one partially sloped at a 12.5 degree angle. Various numbers of Douglas fir timber sets of 0.15 m x 0.15 m (cross section) x 2.4 m (length) were positioned on the two side walls and ceiling of the test section of the horizontal passageway. Number of timber sets used was based on a timber loading density α, defined as the exposed timber surface area (3 sides) per unit flow area of the passageway (excluding the floor). Tests were performed with α = 20, 40, and 80%. In the ignition section of the passageway, various numbers of 0.051 m x 0.051 m (cross section) x 2.4 m (length) Douglas fir wood boards were positioned vertically, close to the two side walls. One 0.5 MW premixed gas burner on each side wall was used to ignite the wood boards. The combination of the wood boards and gas burners served as the ignition source for the timber sets downstream in the passageway. The ignition source intensity could be varied by varying the number of wood boards from 8 to 48. Ventilation air velocities up to 3 m/s were supplied by a constant-speed blower with adjustible blades.

In a typical fire test, an initial cold flow air velocity was selected and set first. The gas burners then ignited the wood boards in the ignition section. Subsequently, the timber sets were ignited and fire propagated downstream toward the exit of the passageway. During the fire, flame spread rate, and gas velocity, temperature and composition were measured in the five measurement stations indicated in Fig. 5.

RESULTS AND DISCUSSION

Model Tunnel Network

Prior to each fire experiment, cold flow characteristics of the single fire duct, the parallel fire and bypass ducts, and the exhaust fan were established. These flow characteristic curves are shown in Fig. 6.

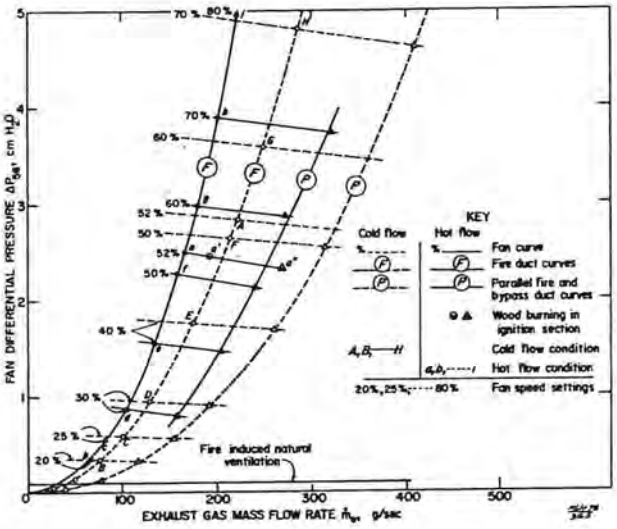

FIGURE 6. Flow characteristics of tunnel network and exhaust fan during cold and hot flows.

To investigate the overall effect of the wood fire on the tunnel ventilation flow, hot flow characteristic curves during the fire were obtained for the single and parallel ducts, and the fan. These curves were generated by measuring the tunnel exhaust mass flow rate and the corresponding fan pressure (or total tunnel pressure drop) at various fan speeds after the wood fire became fully developed. These hot flow characteristic curves together with the cold flow curves are shown in Fig. 6. The cold flow characteristic fan curves were displaced downward during the fire owing to the presence of high temperature gas at the fan. The cold flow curves of the single fire duct and the parallel fire and bypass ducts were shifted toward the left during the fire. These results suggest that the wood fire introduced additional overall flow resistances to the tunnel network. The development of a fire at a constant fan setting of 52% is used to illustrate these results in more detail in Fig. 6. Point A in Fig. 6 corresponds to the equilibrium cold flow condition between the fire duct and the fan at 52% setting. As the burning of the ignition section was established, the fire duct exhaust mass flow rate decreased along the hot flow 52% fan curve to point a'. When the fire became fully developed, the fire duct exhaust mass flow rate further decreased to point a, which was the equilibrium hot flow condition between the fire duct and the fan. Thus, the fire duct exhaust mass flow rate decreased from point A to point a as the fire developed. Similar decreases in exhaust mass flow rate were obtained for other fan speeds, e.g., point E to point e for 40% fan setting as shown in Fig. 6, etc.

Local effects of the fire that contributed to the overall effect on the ventilation flow were investigated by measuring gas mass flow rate, velocity, temperatures, and pressure at six stations: 1 - entrance to fire duct at room condition, 2 - entrance to wood lining in ignition section, 3 - exit of wood lining in test section, 4 - common exit of fire and bypass ducts, 5 - entrance to exhaust fan, and 6 - fan exit. Fig. 7 shows the changes in the pressure drops of the fire duct from cold flow to hot flow as the wood fire developed at a constant fan setting of 52% (see also Fig. 6). It is seen that the available pressure head generated by the fan ΔP_{65} and the pressure drop downstream between the end of the fire zone and the fan entrance ΔP_{35}, remained relatively constant from cold to hot flow as the fire developed. Similarly, the available pressure head for the flow between the duct entrance and the exit of the fire zone ΔP_{13} was also relatively unchanged. However, ΔP_{13} was mostly dissipated in the fire zone as indicated by the opposing paths of ΔP_{12} and ΔP_{23}. Such changes in the pressure drops in and upstream of the fire zone from cold to hot flow indicate the presence of an additional flow resistance in the fire zone that throttled the ventilation air flow. Similar changes in pressure drops from cold to hot flow for other fan settings were also measured. Results are shown in Fig. 8.

The pressure drop measurements are analyzed using the following pressure drop equation for duct flow:

$$\Delta P = f \left(\frac{\rho V^2}{2}\right) \left(\frac{L}{D}\right)^{***} \qquad (1)$$

*** Upper-case letters refer to cold flow condition and lower-case letters refer to hot flow condition, e.g. V versus v.

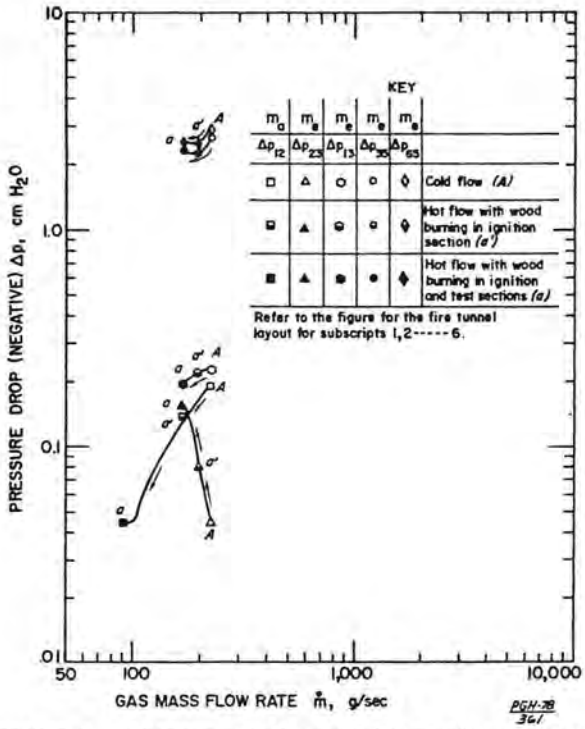

FIGURE 7. Changes of gas mass flow rates and pressures in fire duct of tunnel network from cold to hot flow at constant fan setting of 52% (see Fig. 6).

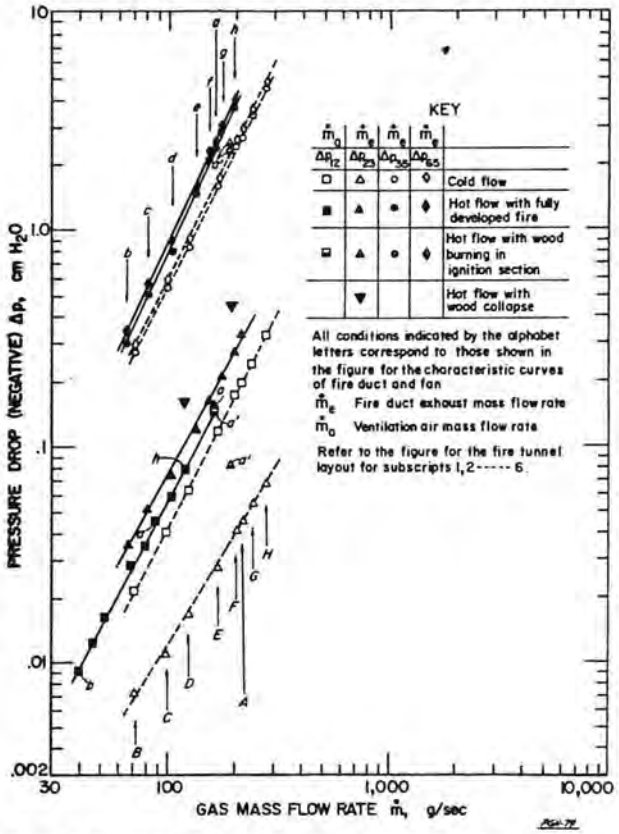

FIGURE 8. Changes of pressure distribution of fire duct in tunnel network from cold to hot flow at different fan settings (see Fig.6).

where f is the duct surface friction coefficient; ρ is the gas density; V is the gas velocity; L is the duct length; and D is the duct hydraulic diameter. Eq. (1) can be rearranged to express ΔP in terms of mass flow rate $\dot{M}$:

$$\Delta P = R\dot{M}^2 \qquad (2)$$

where

$$R = fL/2\rho D^5) \qquad (3)$$

The variable R can be interpreted as the flow resistance of the duct, which is proportional to f and gas temperature. From Eqs. (2) and (3), comparison of ΔP and R between hot and cold flow gives

$$\frac{\Delta p}{\Delta P} = \left(\frac{r}{R}\right)\left(\frac{\dot{m}}{\dot{M}}\right)^2 \qquad (4)$$

$$\frac{r}{R} = \frac{f_h \rho_c}{f_c \rho_h} \qquad (5)$$

where the subscripts h and c refer to hot and cold flow, respectively. Therefore, the change in pressure drop for the same mass flow rate is due to the changes in the wood surface friction coefficient and gas density. Measurements of gas mass flow rate, pressure and temperature in the fire duct, were used to compute the ratios of hot flow resistance to cold flow resistance r/R, based on the same fan setting and the same duct exhaust mass flow rate m_e, across the air inlet duct, the fire zone, and the exhaust duct. Results are shown in Tables 1, 2, and 3. All ratios

TABLE 1 - Comparison of flow resistance of the air intake duct between cold and hot flows.

Hot flow fan setting %	Hot flow $r_{12}\times10^6$ cm $H_2O/(g/sec)^2$	Cold flow* $R_{12,s}\times10^6$ cm $H_2O/(g/sec)^2$	Cold flow* $R_{12,m}\times10^6$ cm $H_2O/(g/sec)^2$	$r_{12}/R_{12,s}$	$r_{12}/R_{12,m}$
20	5.29	3.92	3.93	1.35	1.35
25	5.43	3.83	3.94	1.42	1.38
30	5.45	3.86	3.84	1.41	1.42
40	5.84	3.96	3.99	1.47	1.46
50	5.18	3.90	3.96	1.33	1.31
60	5.56	3.92	5.68	1.42	0.98
70	5.17	4.02	5.44	1.29	0.95

* $R_{12,s}$ and $R_{12,m}$ are the cold flow resistances at the same fan setting and at the same ventilation air mass flow rate as hot flow, respectively (see Fig.8).

TABLE 2 - Comparison of flow resistance of the fire zone between cold and hot flows.

Hot flow fan setting %	Hot flow $r_{23}\times10^6$ cm $H_2O/(g/sec)^2$	Cold flow* $R_{23,s}\times10^6$ cm $H_2O/(g/sec)^2$	Cold flow* $R_{23,m}\times10^6$ cm $H_2O/(g/sec)^2$	$r_{23}/R_{23,s}$	$r_{23}/r_{23,m}$
20	7.61	1.31	1.29	5.81	5.90
25	7.30	1.02	1.22	7.16	5.98
30	6.57	1.03	1.18	6.38	5.57
40	6.37	0.922	1.12	6.91	5.69
50	6.24	0.917	1.03	6.81	6.06
60	6.40	0.896	0.942	7.14	6.79
70	6.45	0.830	0.940	7.77	6.86

* $R_{23,s}$ and $R_{23,m}$ are the cold flow resistances at the same fan setting and at the same duct exhaust mass flow rate as hot flow, respectively (see Fig.8).

TABLE 3 - Comparison of flow resistance of the exhaust duct between cold and hot flows.

Hot flow fan setting %	Hot flow $r_{35} \times 10^5$ cm $H_2O/(g/sec)^2$	Cold flow* $R_{35,s} \times 10^5$ cm $H_2O/(g/sec)^2$	Cold flow* $R_{35,m} \times 10^5$ cm $H_2O/(g/sec)^2$	$r_{35}/R_{35,s}$	$r_{35}/R_{35,m}$
20	6.54	4.93	5.13	1.33	1.27
25	7.11	5.15	5.06	1.38	1.41
30	7.08	5.13	5.37	1.38	1.32
40	7.91	5.32	5.58	1.49	1.42
50	8.45	5.36	5.34	1.58	1.58
60	8.57	5.41	5.33	1.58	1.61
70	8.86	5.5	5.19	1.61	1.71

* $R_{35,s}$ and $R_{35,m}$ are the cold flow resistance at the same fan setting and at the same duct exhaust mass flow rate as hot flow, respectively (see Fig. 8).

of r/R are larger than one, owing to the additional flow resistance introduced by the fire. The largest increase in flow resistance was in the fire zone, i.e., r_{23}/R_{23}. Both r_{23}/R_{23} and r_{35}/R_{35} increased as the fan speed or the exhaust mass flow rate increased. This is because higher fan speeds increased ventilation air flow rate, which in turn intensified the fire and increased the gas temperature. On the other hand, upstream of the fire, as the ventilation air mass flow rate $\dot{m}_a$ increased, r_{12}/R_{12} based on the same $\dot{m}_a$ between cold and hot flow decreased. This is because the temperature field upstream of the fire approached room condition for increasing $\dot{m}_a$.

The pressure drop across the fire zone was investigated in detail using Eqs. (1)-(5). Results are shown in Table 4. It is seen that the friction

TABLE 4 - Comparison of wood surface friction coefficient between cold and hot flows

Hot flow fan setting %	ρ_c/ρ_h	$(\Delta p_{23}/\Delta P_{23})_s^*$	$(f_h/f_c)_s$	$(\Delta p_{23}/\Delta P_{23})_m^*$	$(f_h/f_c)_m$	$(\rho_c/\rho_h)/(f_h/f_c)_m$
20	3.11	4.87	1.87	5.69	1.83	1.70
25	3.28	4.81	2.19	5.95	1.81	1.81
30	3.5	4.37	1.82	6.09	1.74	2.01
40	3.7	4.23	1.86	6.46	1.85	2.0
50	3.83	4.13	1.79	6.48	1.69	2.27
60	3.93	3.78	1.76	6.9	1.76	2.23
70	4.07	3.95	1.90	6.84	1.68	2.42

* Subscript s and m refer to comparisons between hot and cold flow values at constant fan speed and constant duct exhaust mass flow rate, respectively (see Fig. 8).

coefficient increased by about 80% from cold to hot flow. The increase is mostly likely due to the large cracks developing on the wood surface during pyrolysis. Since gas density ρ_h decreased as $\dot{m}_e$ increased, the effect of gas expansion at high temperatures on Δp_{23} exceeded that of the surface friction at high exhaust gas flow rates. These effects are indicated by the values of the ratio $(\rho_c/\rho_h)/(f_h/f_c)$ in Table 4. In addition to the changes in f and ρ as sources for the increase in Δp during the fire, physical plockage of the fallen wood char on the duct gas flow also contributed additional pressure drops, especially in the later stage of the fire. Such additional pressure drops are shown in Fig. 8.

As mentioned before, the ventilation air flow was throttled by the mass and heat generated by the fire. At severe fire throttling, hot gas and smoke from the fire backed into the ventilation air flow, forming a stably stratified reverse flow of hot gas along the ceiling above the colder ventilation air flow. The gas velocity v_t at 0.36 m upstream of the fire and 0.05 m below the duct ceiling were measured and used as an indication of reverse flow. The velocity v_t was correlated with the local Froude number Fr_ℓ at 0.36 m upstream of the fire and the Froude number Fr_a far upstream (room condition) of the fire. These Froude numbers are defined as

$$Fr_\ell \equiv [H(\rho_b-\rho_t)/\rho_b]/(v_b^2/g) \qquad (6)$$

and

$$Fr_a \equiv gH/v_a^2 \qquad (7)$$

In these expressions, H is the tunnel height (0.3 m); ρ_b and ρ_t are the gas densities on the duct floor and ceiling, respectively, where v_b and v_t are measured; v_b is the gas velocity at the same distance from the fire as v_t, and at 0.05 m from the duct floor; g is the gravitational acceleration constant; and v_a is the air velocity far upstream. Basically Fr_ℓ is the local ratio of buoyancy head of the hot gas from the fire to the kinetic head of the ventilation air; and Fr_a is the ratio of buoyancy head of the fire to the kinetic head of the ventilation air far upstream. The density ratio between the fire and the ventilation air has been neglected in Fr_a for simplicity. The Froude numbers are used as criteria for reverse flow. Results in Fig. 9 show that reverse flow occurred at an

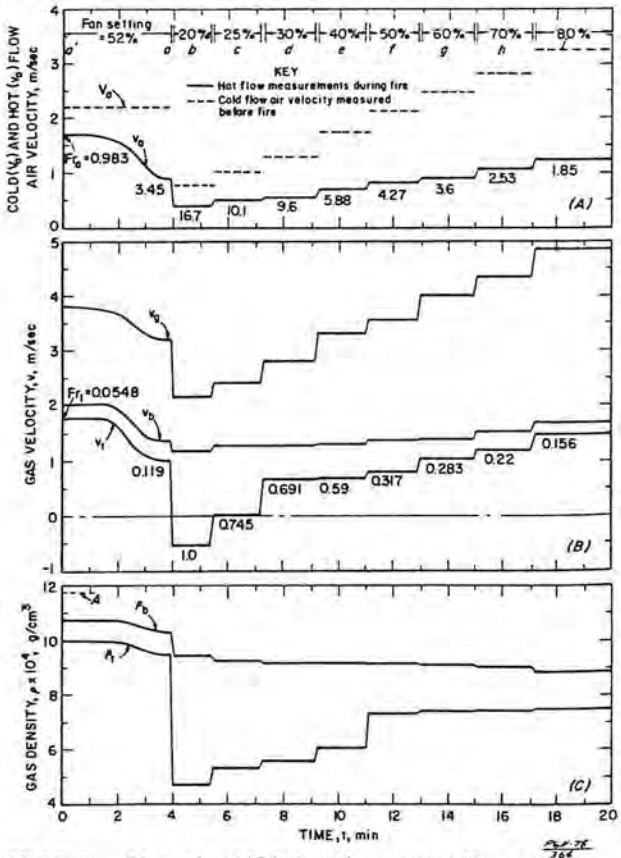

FIGURE 9. Fire throttling and reverse flow measurements in fire duct of tunnel network: A. Changes in ventilation air velocity from cold to hot flow and corresponding Froude numbers, B. Gas velocities upstream of (v_b and v_t) and in (v_g) the fire and local Froude numbers, C. Gas densities upstream of fire.

air velocity of about 0.5 m/s, corresponding to a local Fr_ℓ of about 1 and Fr_a about 10. More detailed study on reverse flow in terms of velocity and temperature distributions upstream of the fire were carried out in the fire-plume tunnel. Results are presented in the next section.

Fire-Plume Tunnel

Since the processes in the model tunnel network were transient in nature, the fire-plume tunnel was constructed to study reverse flow under controlled, steady-state conditions. Figs. 10 and 11 show typical

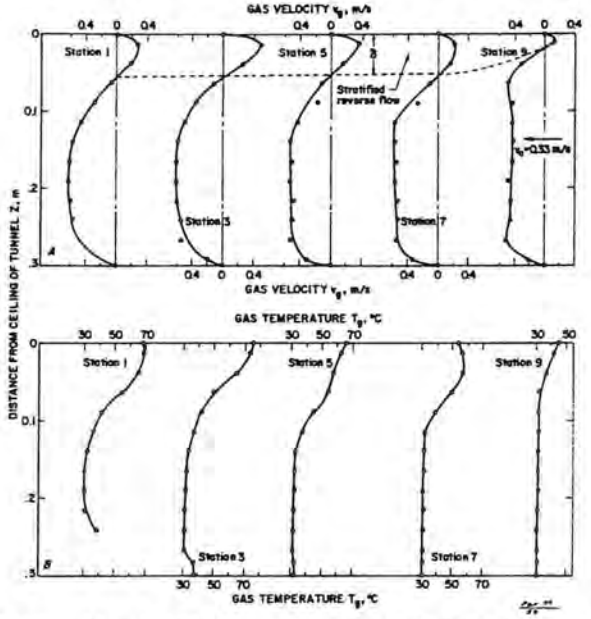

FIGURE 10. Velocity and temperature measurements of one reverse flow in fire-plume tunnel.

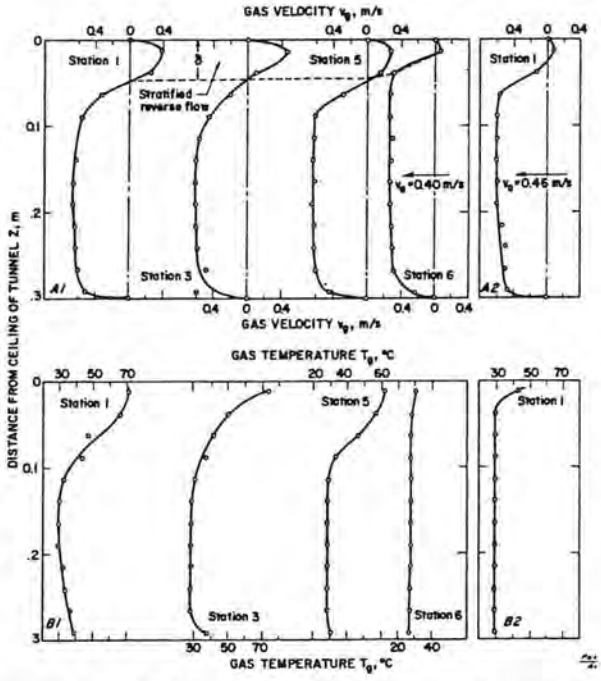

FIGURE 11. Velocity and temperature measurements of two reverse flows in fire-plume tunnel.

velocity and temperature profiles at various measurement stations for three stratified reverse-flow lengths. These three reverse flow conditions were generated using a constant burner setting but different ventilation air velocities as shown in the figures. It is seen that the gas temperatures near the ceiling of the tunnel were higher than those near the floor, and the gas velocities of the top hot layer were in opposite direction to those of the ventilation air near the floor. Except for station 1 near the fire plume, the gas temperatures and velocities of the ventilation air near the floor were quite uniform. Such temperature and velocity distributions characterized the stably stratified reverse flow upstream of the fire plume. The top hot gas layer which extended in both upstream and downstream directions, was fed by the fire plume generated by the gas burners. The flow structure in the vicinity of the plume (station 1 was basically three-dimensional owing to flow interaction between the rising hot plume and the forced ventilation air flow. However, upstream in the stratified reverse flow region, the flow structure was essentially two-dimensional, as evidenced by the movement of the smoke particles injected through the ceiling near the fire plume.

As shown in Figs. 10 and 11, the thickness of the reverse flow layer δ gradually decreased from the fire plume toward the end of the reverse flow. Near the end of the layer, the velocity changed quite abruptly to zero, generally within a distance of 2-3 δ. The length of the reverse flow ℓ was quite sensitive to the ventilation air velocity v_a and varied inversely to it as expected. Both ℓ and δ increased as v_a decreased.

The reverse flow measurements in Figs. 10 and 11 are correlated using the two Froude numbers Fr_ℓ and Fr_a previously defined. Results are shown in Fig. 12.

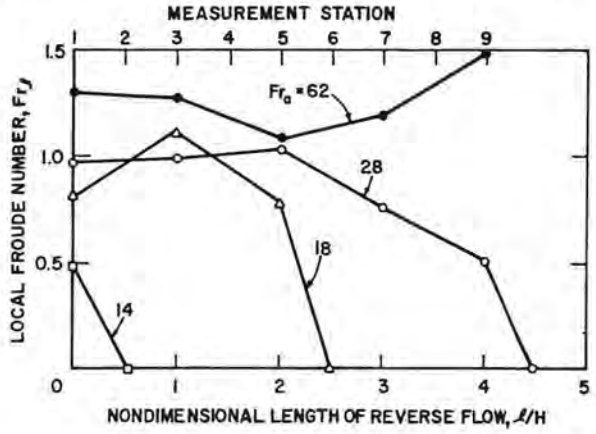

FIGURE 12. Variation of reverse flow length with respect to Froude numbers Fr_ℓ and Fr_a.

Except for the longest layer (not shown in Figs. 10 and 11) which extended beyond station 9 in the test section of the tunnel, Fr_ℓ decreased with the distance from the fire plume, indicating a decreasing buoyancy head of the hot layer as compared to the kinetic head of the ventilation air. As expected, a larger initial value of Fr_ℓ correlates with a longer reverse flow length. Of all the four reverse flow lengths, values of Fr_ℓ were all greater than, or of order of 1.0 upstream of the reverse flow near the fire plume. Such values are consistent with the

results obtained earlier in the fire duct of the model tunnel network.

As indicated in Figs. 10 and 11, the ventilation air was heated as it approached from the tunnel entrance to the fire plume. Consequently, the ventilation air velocity increased from v_a to v_b near the fire plume. In a real mine fire situation, v_a is often more accessible for measurement than v_b. Therefore, it is more convenient to use Fr_a, which is based on v_a, as a criterion for reverse flow. It is seen from Fig. 12 that reverse flow began to occur when Fr_a was of an order of 10. This is again consistent with the results obtained in the fire duct of the model tunnel network. As expected, reverse flow length increased as Fr_a increased or v_a decreased.

In general, the results from both the fire-plume tunnel and the model tunnel network give approximately the same criteria of $Fr_\ell \approx 1$ and $Fr_a \approx 10$ for reverse flow. The range of density ρ in the tunnels covers from 1.18 to 0.3 kg/m^3 which may exist in passageway fires in mines. It should be recognized that the Froude number Fr_a is based on the air velocity v_a during a fire. As shown previously, the cold flow air velocity V_a is throttled to v_a during a fire. The amount of throttling is a function of fire intensity and flow characteristics of the tunnel network and the fan. To avoid reverse flow, it is important to be able to predict the value of V_a before a fire so that the corresponding v_a during the fire will be high enough to suppress reverse flow. Such a task requires flow network analysis of the passageways utilizing the criteria of Fr_ℓ and Fr_a as presently determined and the characteristics of the fire. Such an analysis for the model tunnel network has already been performed for the model tunnel network by Lee et al[3].

It should be further recognized that the criteria of Fr_ℓ and Fr_a for reverse flow as determined should be verified in large-scale passageway fires to demonstrate their practical utility. Such large-scale fires are discussed in the next section.

Simulated Mine Gallery

Some of the results on fire throttling from the timber-set fire tests in the large-scale simulated mine gallery are shown in Table 5 (more complete

TABLE 5 - Mass flow rates before and during timber-set tests in the simulated mine gallery.

Timber loading density α, %	$\dot{M}_a$ kg/s	$\dot{m}_a$ kg/s	$\dot{m}_g$ kg/s	$\dot{m}_t$ kg/s	$\dot{m}_e$ kg/s	$\dot{m}_a/\dot{M}_a$ -	$\dot{m}_e/\dot{M}_a$ -
20	8.4	4.9	2.22	0.776	7.89	0.583	0.939
	18.5	13.0	2.23	1.21	16.4	0.703	0.886
40	9.0	4.8	2.26	0.593	7.65	0.533	0.85
	17.6	12.6	2.29	0.924	15.8	0.716	0.898
80	9.0	4.5	2.28	1.95	8.73	0.5	0.97
	19.1	11.5	2.27	1.94	15.7	0.602	0.822

results will be presented by Croce et al[7]). Results in Table 5 are given in terms of cold and hot ventilation air mass flow rates $\dot{M}_a$ and $\dot{m}_a$, respectively, mass flow rate from the two burners $\dot{m}_g$, fuel mass generation rate from timber sets $\dot{m}_t$, and hot flow gallery exhaust mass flow rate $\dot{m}_e$($\dot{m}_e = \dot{m}_a+\dot{m}_g+\dot{m}_t$). These measurements were made during active burning of the timber sets for three values of timber-set loading density α of 20%, 40% and 80%. For each α, two values of $\dot{M}_a$, corresponding to ventilation air velocities of 1.5 m/s and 3.0 m/s, were used.

It is seen from Table 5 that $\dot{M}_a$ was throttled to lower values of $\dot{m}_a$ owing to the fire. The amount of decrease was as high as 50%. The degree of fire throttling decreased as $\dot{M}_a$ increased for a fixed α. This is because higher $\dot{M}_a$ decreased the gas temperature owing to oxygen-rich burning of the fire. On the other hand, it was found previously that higher $\dot{M}_a$ increased the gas temperature and fire throttling in the model tunnel network owing to fuel-rich burning of the fire. Gallery exhaust mass flow rate decreased during the fire as expected. The decrease was due to the increased flow resistance of the gallery generated by the fire.

Hot flow ventilation air velocity v_a necessary to suppress reverse flow in the full-scale gallery was estimated using the critical Froude number Fr_a of 10 determined in the two small-scale fire tunnels. Value of v_a was calculated to be 1.5 m/s. Test results in the gallery show that reverse flow occurred at V_a = 1.5 m/s[6]. The cold flow air velocity V_a was throttled to approximately 0.5 V_a with v_a about 0.7 m/s, a value lower than 1.5 m/s. Such comparison between the small- and large-scale fires indicates favorable utility of using Fr_a as a criterion for reverse flow. However, it should be noted that more detailed study on reverse flow in large-scale passageway fires and flow analysis of reverse flow are necessary to demonstrate the Froude number scaling concept and to elucidate the basic phenomena of reverse flow. These studies are presently underway at the Pittsburgh Research Center.

CONCLUSION

The present study demonstrates the complex interaction among a passageway fire, ventilation air flow, and the fan in a tunnel flow network. The study is particularly applicable to ventilation and fires in underground mines. It is the heat and mass addition from the fire into the ventilation gas stream that disturbs the cold flow equilibrium operating condition of the network. The disturbance results in an overall increase in the flow resistance of the network and leads to throttling of the ventilation air in a moderate fire situation and reverse flow in a serious situation. Such changes in the ventilation flow pattern in a mine could result in an extremely hazardous situation. The changes can be predicted only by means of a thorough flow network analysis of the entire flow system that includes fire characteristics in terms of fuel mass injection rate and combustion temperatures, and reverse flow criteria such as the Froude numbers as input information to the analysis. The concepts and findings reported in this paper should find application in establishing guidelines for planning and control of ventilation flows in the event of mine fires.

SECOND INTERNATIONAL MINE VENTILATION CONGRESS

Reno, NV, November 4-8, 1979

Pierre Mousset-Jones
Professor of Mining Engineering
Editor

Sponsored by

Mackay School of Mines, University of Nevada-Reno
Mine Safety & Health Administration, US Department of Labor

Society of Mining Engineers
of
American Institute of Mining, Metallurgical, and Petroleum Engineers, Inc.
New York • 1980